Journal of Nuclear and Radiochemical Sciences, Vol. 10, No.1, pp. 19-26, 2009

Heat Capacity and Thermal Expansion of Uranium-Gadolinium Mixed Oxides

R. Venkata Krishnan, G. Panneerselvam, P. Manikandan, M.P. Antony, and K. Nagarajan*

Fuel Chemistry Division, Indira Gandhi Centre for Atomic Research, Kalpakkam-603 102, Tamil Nadu, India

Received: January 16, 2009; In Final Form: May 15, 2009

Uranium-gadolinium mixed oxides of four different compositions, $(U_{1-y}\ Gd_y)\ O_{2\pm x}$ (y = 0.1, 0.2, 0.5, and 0.8), were synthesized. Single-phase fluorite structure was observed for the compositions $(U_{1-y}\ Gd_y)\ O_{2\pm x}$ (y = 0.1, 0.2, and 0.5). The room temperature lattice constants measured for $(U_{0.9}\ Gd_{0.1})\ O_{2.02}$, $(U_{0.8}\ Gd_{0.2})\ O_{2.00}$, and $(U_{0.5}\ Gd_{0.5})\ O_{1.98}$ are 0.5463, 0.5454, and 0.5433 nm, respectively. Heat capacity measurements in the temperature range 298 – 800 K were carried out using a differential scanning calorimetry. Considerable anomalous increases in the heat capacity values were observed for compositions $(U_{1-y}\ Gd_y)\ O_{2\pm x}$ with y = 0.1, 0.2, and 0.5. The heat capacity values of $(U_{0.9}\ Gd_{0.1})\ O_{2.02}$, $(U_{0.8}\ Gd_{0.2})\ O_{2.00}$, and $(U_{0.5}\ Gd_{0.5})\ O_{1.98}$ at 298 K are 63.5, 61.1, and 65.7, respectively. Thermal expansion characteristics of $(U_{0.9}\ Gd_{0.1})\ O_{2.02}$, $(U_{0.8}\ Gd_{0.2})\ O_{2.00}$, and $(U_{0.5}\ Gd_{0.5})\ O_{1.98}$ were studied using a high temperature X-ray diffraction in the temperature range 298 – 1973 K.

1. Introduction

Gadolinium is one of the major fission products and its oxide forms solid solutions with uranium. Thermodynamic properties, such as heat capacity, Gibbs free energy etc, of the (U, Gd) oxides are required for understanding the oxide fuel behaviour during irradiation and also to understand the chemical state of gadolinium in the fuel.

It has been observed[1,2] that the heat capacity of UO_2 increases rapidly from about 1500 K and becomes more than twice the Dulong-Petit value near the melting temperature. This anomalous behavior has been given various interpretation as due to formation of Frenkel pairs of oxygen,[3] electronic excitation[4-6] etc. It will be interesting to check whether (U, Gd) O_2 solid solution also shows anomalous increase in heat capacity like UO_2. Considerable discrepancy has been found in the literature regarding the high temperature heat capacity anomalies observed for Gd doped UO_2. Inaba et al[7] measured heat capacities of UO_2 doped with $GdO_{1.5}$ with Gd contents ranging from 4.4 to 14.2 mol% by direct heating pulse calorimetry and reported anomalous steep increase in the heat capacity with onset temperatures ranging from 800 to 1200 K. They also reported that the onset temperature of heat capacity anomaly decreases with increase in Gd content. Arita et al[8] and Matsui et al[9-11] have also made similar observations on their measurements regarding the heat capacity of uranium oxide doped with oxides of lanthanides obtained by direct heating pulse calorimetry.

Amaya et al[12,13] measured the heat capacity of (U, Gd) O_2 with Gd contents ranging from 0 to 27% by differential scanning calorimetry in the temperature range 325 to 1673 K and reported no anomalous increase in the heat capacity in the temperature range of measurement. Takahashi et al[14] measured the heat capacity of UO_2 doped with Gd_2O_3 ranging from 7.5 mol% to 14.2 mol% using drop calorimetry in the temperature range 400 – 1500 K and reported that such thermal anomalies were not found in the heat capacities. They also reported that the heat-capacity values are close to the ones computed using Neumann-Kopp's law, whereas the measured heat capacity values of Amaya et al are 3 – 4% lower than the values computed using Neumann-Kopp's additivity rule. The aim of the present study is to investigate the existing discrepancy in the literature data. Measurements of heat capacities of $(U_{1-y}\ Gd_y)\ O_{2\pm x}$ (y = 0.1, 0.2, and 0.5) were carried out using differential scanning calorimeter in the temperature range 298 – 800 K.

To the best of our knowledge, high temperature X-ray diffraction (HTXRD) based lattice thermal expansion data for (U, Gd) mixed oxides are not available in the literature. Therefore, HTXRD based thermal expansion measurements were performed on $(U_{1-y}\ Gd_y)\ O_{2\pm x}$ (y = 0.1, 0.2, and 0.5) in the temperature range 298 to 1973 K. The results of the heat capacity and thermal expansion measurements are discussed in this paper.

2. Experimental

2.1. Sample preparation. UO_2 of nuclear grade purity supplied by Nuclear Fuel Complex, Hyderabad and Gd_2O_3 of 99.9% purity supplied by M/s. Indian Rare Earths were used for preparing the samples. Solid solutions of $(U_{1-y}\ Gd_y)\ O_{2\pm x}$ were prepared by combustion synthesis using citric acid as fuel. UO_2 was heated in air at 873 K for 6 h to convert it to U_3O_8. Gd_2O_3 was heated in air at 673 K to remove any adsorbed moisture. Stiochiometric amounts of U_3O_8 and Gd_2O_3 were taken and dissolved in nitric acid by heating at around 353 K. Citric acid was then added to the nitrate solution and mixed to get a clear solution. The mixture was then heated on a hot plate at 673 K. Combustion of the mixture took place with a flame. The resultant fine powder was calcined at 1073 K in air for 4 h to remove carbonaceous material from the sample. The resultant fine powder was compacted into pellets of 5 mm diameter using a hydraulic press. The pellets were heated at 1873 K in a tungsten mesh furnace for 6 h. Before heating the samples, the furnace was evacuated to 10^{-3} mbar and filled with ultra high pure Ar+8% H_2 gas mixture three times. The heating of the sample pellets was done under flowing Ar+8% H_2 gas mixture. The samples prepared were stored in an argon atmosphere glove box containing less than 20 ppm of moisture and oxygen to prevent oxidation of the sample.

2.2. Sample characterization.

2.2.1. Compositional characterization. The composition of U and Gd in the samples was determined by high performance liquid chromatography (HPLC) and inductively coupled plasma atomic emission spectroscopy (ICP-AES) technique.

HPLC technique. A Jasco model HPLC system was used in the present study. The instrument consists of a sample injector

*Corresponding author. E-mail: knag@igcar.gov.in Fax: (+91) 44-27480065

Published on Web 06/30/2009

(Rheodyne, 20 μL sample loop), reverse phase C18 column, and a UV-visible spectrophotometric detector. The signal from the detector is processed using Borwin software for peak area, peak height, and retention time measurements. U and Gd in the samples were detected by a post-column derivitisation technique using arsenazo (III) as the post-column complexing agent and the complexes were monitored at 665 nm. Solution of α-hydroxy isobutyric acid (HIBA) in 7% methanol was used as the eluent for the separation of metal ions. The pH of the mobile phase was adjusted to 3 with dilute ammonia. Standard samples of U and Gd was initially prepared by dissolving stoichiometric quantities of U_3O_8 and Gd_2O_3 in nitric acid and diluting to a concentration range of 5 – 100 ppm. Similarly mixed oxide samples were also dissolved in nitric acid and diluted. The concentration of U and Gd in the samples was determined from the calibration plots of the standard samples.

ICP-AES technique. Standard samples of U and Gd in the range of 5 – 25 ppm were prepared as explained above. The wavelengths used for U and Gd detection were 385.958 nm and 342.247 nm, respectively. The concentration of U and Gd in the samples was determined using calibration plots.

2.2.2. Structural Characterization. Pellets of ($U_{0.9}Gd_{0.1}$), ($U_{0.8}Gd_{0.2}$), ($U_{0.5}Gd_{0.5}$), and ($U_{0.2}Gd_{0.8}$) mixed oxides as well as those of pure Gd_2O_3 and $UO_{2.00}$ from the same lot used for a differential scanning calorimetry (DSC) measurements were powdered and characterized by X-ray diffraction (XRD). The XRD patterns were recorded in the range, $10°<2\theta<80°$. Peak positions and the relative intensities were computed using a peak-fit program of the Philips X'pert Plus® software. The calibration of the diffractometer was carried out using silicon and α-alumina standards. The XRD patterns of Gd_2O_3 and $UO_{2.00}$ agree well with the literature data.[15,16]

The room temperature XRD patterns of UO_2, Gd_2O_3, and $(U_{1-y}Gd_y)O_{2\pm x}$ (y = 0.1 – 0.8) are shown in Figure 1. The lattice parameter (a) in each case was estimated by considering the eight major reflections of the CaF_2 structure. Finally an effective high angle corrected lattice parameter at each temperature was obtained by the standard Nelson-Riley extrapolation procedure. The solid solutions $(U_{1-y}Gd_y)O_{2\pm x}$ (y = 0.1, 0.2, and 0.5) prepared have a well crystallized single phase fluorite structure, whereas $(U_{0.2}Gd_{0.8})O_{1.71}$ showed in addition faint hexagonal Gadolinia lines (HGD).[17] Beals et al[18] also made similar observation and reported that in $(U_{1-y}Gd_y)O_{2\pm x}$ system, single phase fluorite-type structure was observed until for y = 0.54 but an additional monoclinic Gd_2O_3 phase was present in solid solution containing higher Gd. However, in the present study the additional phase is hexagonal Gd_2O_3. In the reported pseudo-binary phase diagram of $UO_2 – GdO_{1.5}$ by Aitken et al,[19] a hexagonal phase of composition corresponding to $UO_2{\cdot}3Gd_2O_3$ has been reported. But in our samples and also in the study of Beals et al,[18] no such hexagonal phase was observed. The room temperature lattice parameter of UO_2, Gd_2O_3, $(U_{0.9}Gd_{0.1})O_{2.02}$, $(U_{0.8}Gd_{0.2})O_{2.00}$, and $(U_{0.5}Gd_{0.5})O_{1.98}$ are given in Table 1.

2.2.3. Determination of O/M ratio. The O/M ratios of the mixed oxides were determined by spectrophotometric method.[20] The urania-gadolinia samples were dissolved in concentrated phosphoric acid (2 – 3 mg/mL). U^{4+} was determined by absorbance at 540 nm and U^{6+} by absorption at 315 nm.[14] Assuming that the Gd in the solid solution is present only in +3 state and oxygen in –2 state, the O/U ratio was determined as follows.

$$O/U = (3n_{U(VI)} + 2n_{U(IV)}) / (n_{U(VI)} + n_{U(IV)}) \quad (1)$$

where $n_{U(VI)}$ and $n_{U(IV)}$ are number of moles of U(VI) and U(IV), respectively. The O/M of $(U_{1-y}Gd_y)O_{2\pm x}$ is calculated as follows

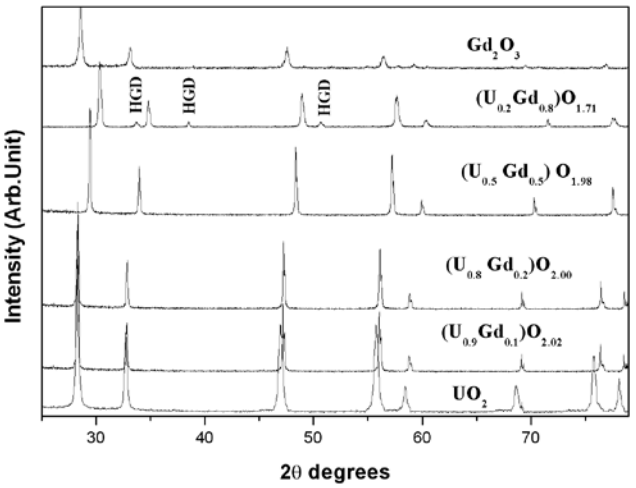

Figure 1. Room temperature XRD patterns of UO_2, Gd_2O_3, and $(U_{1-y}Gd_y)O_{2\pm x}$.

TABLE 1: X-ray and chemical analysis of urania-gadolinia solid solutions

Compound	O/U	O/M	Lattice parameter (nm)	Phases present
$UO_{2.00}$	2.00	2.00	0.5468	FCC
Gd_2O_3	-	1.50	0.5396	FCC
$(U_{0.9}Gd_{0.1})O_{2.02}$	2.07	2.02	0.5463	FCC
$(U_{0.8}Gd_{0.2})O_{2.00}$	2.13	2.00	0.5454	FCC
$(U_{0.5}Gd_{0.5})O_{1.98}$	2.47	1.98	0.5433	FCC
$(U_{0.2}Gd_{0.8})O_{1.71}$	2.53	1.71		FCC+ Hexagonal Gadolinia (HGD)

$$O/M = (1 - y)(O/U) + 1.5\,y \quad (2)$$

The estimated O/M, lattice parameter and the phases present in the solid solution are listed in Table 1.

2.3. Calorimetric measurements. A heat flux type differential scanning calorimeter, model number DSC821e/700 of M/s. Mettler Toledo GmbH, Switzerland was used in this study. Temperature, heat, and τ-lag calibrations were carried out as explained in our previous publication.[21] Heat rate calibration was performed prior to each heat capacity measurement with a disc of sapphire supplied by M/s. Mettler Toledo GmbH and using the heat capacity data of sapphire from NIST, USA. Heat capacity measurements were carried out in the temperature range 298 – 800 K. To remove any adsorbed moisture on the sample, the samples were heated to 573 K before starting the experiment. About 100 – 150 mg of samples in the form of pellet were weighed accurately and hermetically sealed in 40 µL Al-pans. The flow rate of the purge gas (ultra high pure argon) was 50 mL min^{-1}. A three segment-heating program, as explained in our previous work,[21] was used for heat capacity measurements. Each heat capacity measurement consisted of three runs, namely, a blank run with empty pans on the sample and the reference sides, a sapphire run with empty pan on the reference side and a pan with sapphire on the sample side, and finally a sample run with empty pan on the reference side and the pan with sample on the sample side.

2.4. Thermal expansion studies. The thermal expansion characteristics of the samples were studied using HTXRD in the temperature range 298 – 1973 K. The HTXRD studies

were performed in a Philips-X'pert MPD® system equipped with the Büehler® high vacuum heating stage. Typical instrument related parameters were: operating voltage of 40 kV; current of 45 mA for the X-ray tube; scan speed of 0.02° s^{-1} with a counting time of 6 s per step; an angular range (2θ) of 20 to 80°. The heating stage consisted of a thin (~80 μm), heat-resistant tantalum foil, on top of which the sample was placed. The temperature was measured by a W-Re thermocouple, which was spot-welded to the bottom of the tantalum heater. The temperature was controlled to an accuracy of about ± 1 K. Diffraction studies were performed using *CuK*α radiation in the Bragg-Brentano geometry in steps of 100 K up to 1973 K. A heating rate of 1 K min^{-1} and a holding time of 60 min at each temperature of measurement were adopted. The specimen stage was purged with high purity helium three times before the start of every experimental run and a vacuum level of about 10^{-5} mbar was maintained throughout the experiment. Acquisition and preliminary analysis of data were performed by the Philips X'pert Plus® software, although at a latter stage, an independent processing of the raw data for a precise determination of the peak position was resorted to. Room temperature XRD pattern was again taken after the completion of thermal expansion measurements to confirm that no oxidation of the sample had taken place during measurement.

3. Results

3.1. Heat capacity of Gd_2O_3 and UO_2. Heat capacity of UO_2 was measured and reported in our previous publication.[21] Heat capacity values of Gd_2O_3 measured by DSC in the present work and given in Table 2 are the mean of nine measurements. The relative standard deviations are in the range of 1 – 3%. The measured heat capacity data of Gd_2O_3 were fitted to obtain the following polynomial in temperature by the least squares method.

$$C_{p,m}\,(\mathrm{J\,K^{-1}\,mol^{-1}}) = 109.53 + 0.0259\,T - 734459.87\,T^{-2} \quad (298 - 820) \qquad (3)$$

The standard error of the fit is 0.9 J K^{-1} mol^{-1}. The measured data along with the fit values are shown in Figure 2. The heat capacity data of Gd_2O_3 reported in the literature[22] are also shown in Figure 2. As can be seen, the present data are 1 – 3% higher than that of the recommended values of Pankratz.[22] Konings et al[23] measured low temperature (4 – 380 K) heat capacity of monoclinic Gd_2O_3 using an adiabatic calorimeter. The present value of $C_{p,m}$ at 298 K of Gd_2O_3 (109.8 J K^{-1} mol^{-1}) is about 2% higher than that of Konings et al (108.1 J K^{-1} mol^{-1}).[23]

3.2. Heat capacity of $(U_{1-y}\,Gd_y)\,O_{2\pm x}$. Heat capacity of $(U_{1-y}\,Gd_y)\,O_{2\pm x}$ (y = 0.1, 0.2, and 0.5) measured by DSC in the present work and given in Table 3 – 5 respectively are the mean of nine measurements. The fitting equations along with the relative standard deviations are given in Table 6. The measured heat capacity values of the three different mixed oxide samples were fitted to obtain the polynomial in temperature by a least squares method. The standard errors of the fits are also listed in Table 6. The measured heat capacity of the mixed oxides along with the fitting results is shown in Figures 3 – 5. The heat capacity data estimated by Neumann-Kopp's law using the present heat capacity data of Gd_2O_3 and the literature heat capacity data[24] of UO_2 are also given in Figures 3 – 5. The corrections in the heat capacity values for non-stoichiometry were made using the method described by Mills et al.[25]

$$C_{p,m}\,(UO_2) = [(3 / (3 + x)]\,C_{p,m}\,(UO_{2+x}) \qquad (4)$$

From the heat capacity data other thermodynamic functions such as enthalpy, entropy, and Gibbs energy functions were computed and given in Table 3 – 5. The S_{298} data of $(U_{1-y}\,Gd_y)$

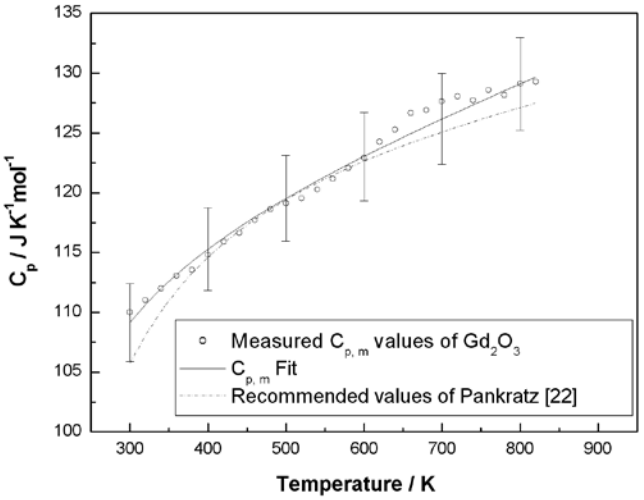

Figure 2. Heat capacity data of Gd_2O_3.

TABLE 2: Heat capacity data of Gd_2O_3

T (K)	$C_{p,m}$ (J K^{-1} mol^{-1})		
	Measured	Fit	Literature value[22]
298	109.8	109.0	105.49
300	110.0	109.1	105.75
400	114.8	115.3	114.63
500	119.1	119.5	119.43
600	122.9	123.0	122.64
700	127.6	126.2	125.08
800	129.1	129.1	127.12

TABLE 3: Thermodynamic functions for $(U_{0.9}\,Gd_{0.1})\,O_{2.02}$

T(K)	$C_{p,m}$ (J K^{-1} mol^{-1})		$H_T - H_{298}$	S_T	$G_T - H_{298}/T$
	Measured	Fit	(J mol^{-1})	(J K^{-1} mol^{-1})	(J K^{-1} mol^{-1})
298	63.5	63.2	0	78.5	-78.5
300	64.1	63.6	127	78.9	-78.5
400	72.5	73.1	7041	98.7	-81.1
500	76.3	76.7	14541	115.5	-86.4
600	79.2	79.3	22322	129.7	-92.5
700	82.6	82.4	30368	142.1	-98.7
800	85.4	86.7	38769	153.4	-104.9

TABLE 4: Thermodynamic functions for $(U_{0.8}\,Gd_{0.2})\,O_{2.00}$

T(K)	$C_{p,m}$ (J K^{-1} mol^{-1})		$H_T - H_{298}$	S_T	$G_T - H_{298}/T$
	Measured	Fit	(J mol^{-1})	(J K^{-1} mol^{-1})	(J K^{-1} mol^{-1})
298	61.1	61.1	0	79.3	-79.3
300	61.9	61.3	122	79.8	-79.3
400	66.6	66.8	6566	98.3	-81.9
500	69.8	69.1	13350	113.5	-86.8
600	71.5	71.4	20341	126.3	-92.4
700	74.9	74.7	27594	137.5	-98.1
800	79.8	79.5	35237	147.8	-103.7

TABLE 5: Thermodynamic functions for ($U_{0.5}$ $Gd_{0.5}$) $O_{1.98}$

T(K)	$C_{p,m}$ (J K^{-1} mol^{-1})		$H_T - H_{298}$	S_T	$G_T - H_{298}/T$
	Measured	Fit	(J mol^{-1})	(J K^{-1} mol^{-1})	(J K^{-1} mol^{-1})
298	65.7	65.7	0	82.2	-82.2
300	66.1	65.8	131	82.6	-82.2
400	69.1	69.5	6927	102.2	-84.9
500	69.6	70.3	13899	117.8	-90.0
600	70.0	71.3	20940	130.7	-95.8
700	72.0	73.4	28115	141.8	-101.7
800	75.1	77.0	35558	151.8	-107.4

$O_{2\pm x}$ required for the computation of entropies were estimated by Neumann-Kopp's law using the literature data of S^0_{298} of pure Gd_2O_3[22] and UO_2[24] including the contribution of entropy of mixing.

3.3. Thermal expansion measurements.

3.3.1. Thermal expansion measurements of UO_2 and Gd_2O_3. Both UO_2 and Gd_2O_3 have face centered cubic (fcc) lattice. For fcc lattice, the lattice parameter a is related to the d-spacing by the following equitation

$$d = \frac{a}{\sqrt{h^2 + k^2 + l^2}} \quad (5)$$

where h, k, l are the Millar indices of the plane. The room temperature cubic lattice parameter obtained for UO_2 and Gd_2O_3 are 0.5470 and 0.5396 nm, respectively. The room temperature lattice parameters obtained in the present study are in good agreement with the literature value.[15,16] Room temperature XRD patterns for pure UO_2 and Gd_2O_3 are given in Figure 1. The measured temperature dependence of the lattice parameter in the temperature range 298 – 1973 K for UO_2 and Gd_2O_3 are presented in Figure 6. The variation of lattice parameter, a (nm) with temperature (K) for UO_2 and Gd_2O_3 is fitted to a second order polynomial in the temperature interval (T-298) by least squares and are given by the following expression

$$a(\text{nm})\ (UO_2) = 0.5458 + 3.0348 \times 10^{-6}\ (T - 298) + 1.4419 \times 10^{-10}\ (T - 298)^2 \quad (6)$$

$$a(\text{nm})\ (Gd_2O_3) = 0.5391 + 1.3531 \times 10^{-6}\ (T - 298) + 1.1532 \times 10^{-10}\ (T - 298)^2 \quad (7)$$

Equations 6 and 7 are used to calculate the mean linear thermal expansivities and are presented in Table 7. The percentage linear thermal expansions calculated from corrected lattice parameters are fitted in to second order polynomial and the expressions are presented below.

$$\text{Thermal Expansion (\%)}\ (UO_2) = -0.20588 + 6.1209 \times 10^{-4}\,T + 2.6361 \times 10^{-7}\,T^2\ (298 - 1973) \quad (8)$$

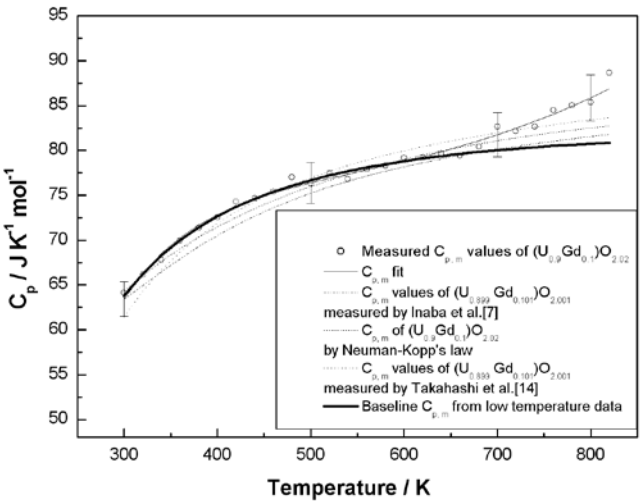

Figure 3. Heat capacity data of ($U_{0.9}$ $Gd_{0.1}$) $O_{2.02}$.

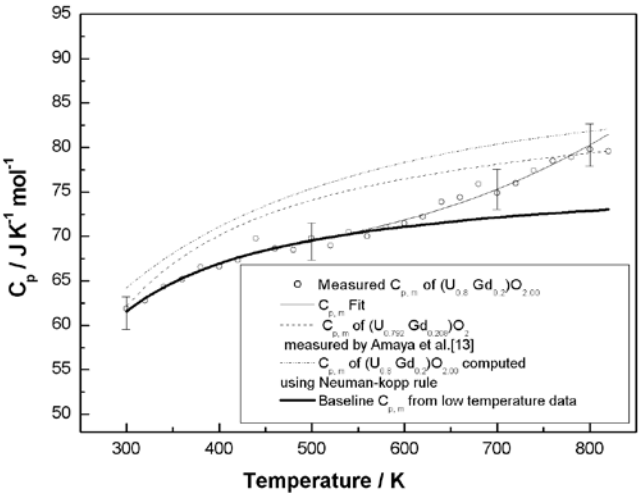

Figure 4. Heat capacity data of ($U_{0.8}$ $Gd_{0.2}$) $O_{2.00}$.

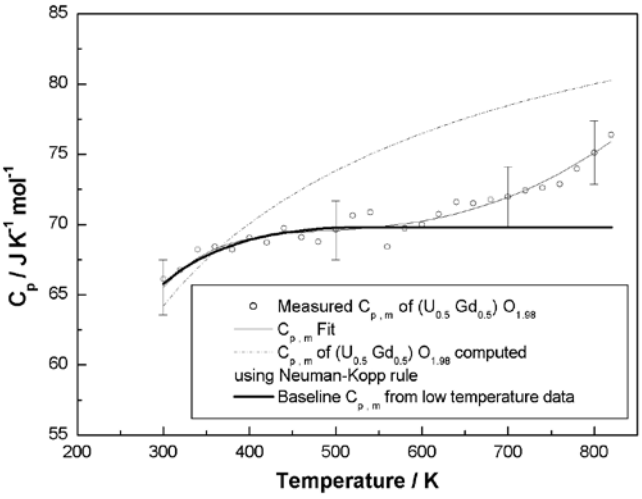

Figure 5. Heat capacity data of ($U_{0.5}$ $Gd_{0.5}$) $O_{1.98}$.

TABLE 6: Fitting equations of the measured heat capacity data (298 ≤ T/K ≤800)

No.	Compound	Fitting equation (J K^{-1} mol^{-1})	Standard deviation	Standard error J K^{-1} mol^{-1}
1	($U_{0.9}$ $Gd_{0.1}$) $O_{2.02}$	124.364 – 0.1213 T – 3009415 T^{-2} + 0.0001 T^2	1 – 2%	0.67
2	($U_{0.8}$ $Gd_{0.2}$) $O_{2.00}$	107.88 – 0.11156 T – 1992751 T^{-2} + 0.0001 T^2	1 – 2%	0.77
3	($U_{0.5}$ $Gd_{0.5}$) $O_{1.98}$	114.0413 – 0.12273 T – 1837744 T^{-2} + 0.0001 T^2	1 – 2%	0.64

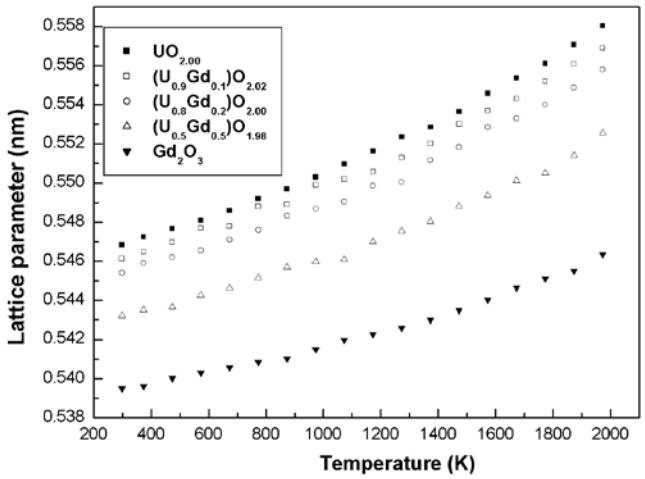

Figure 6. Lattice parameter as function of temperature of UO_2, Gd_2O_3, and (U_{1-y} Gd_y) $O_{2\pm x}$ (y = 0.1, 0.2, and 0.5).

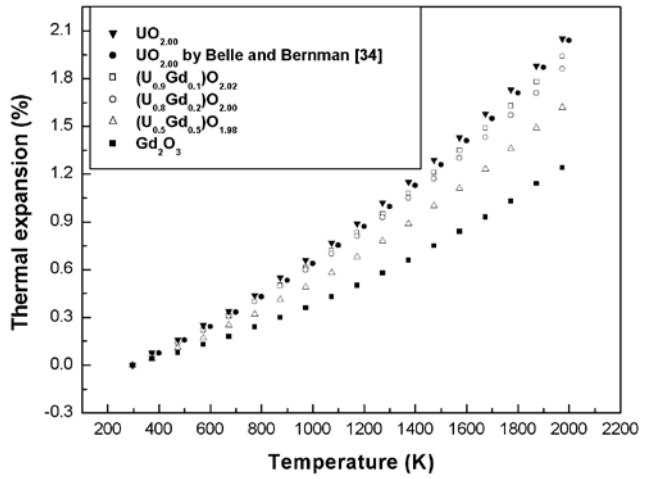

Figure 7. Thermal expansion data of UO_2, Gd_2O_3, and (U_{1-y} Gd_y) $O_{2\pm x}$ (y = 0.1, 0.2, and 0.5).

$$\text{Thermal Expansion (\%) } (Gd_2O_3) = -0.09378 + 2.5077 \times 10^{-4}\,T + 2.1372 \times 10^{-7}\,T^2 \quad (298 - 1973) \qquad (9)$$

The percentage linear thermal expansion of UO_2 and Gd_2O_3 computed from the above fitting equations are presented in Table 7 and are also shown in Figure 7. Good amount of work regarding thermal expansion of urania have been carried out.[26-33] Based on them Belle and Berman[34] arrived at a recommended value of thermal expansion characteristics of UO_2. The percentage thermal expansion data of UO_2 obtained in the present study as well as by Belle and Berman[34] are illustrated in Figure 7 as a function of temperature. The measured % thermal expansion is in good agreement with the values recommended by Belle and Berman[34] within ±1%. The % linear thermal expansion value measured in the present study in the temperature range from 298 to 1973 K is 2.03; this value compares with 2.04, the recommended values for UO_2 by Belle and Berman.[34]

3.3.2. Thermal expansion measurements on (U_{1-y} Gd_y) $O_{2\pm x}$. The measured lattice parameters of ($U_{0.9}$ $Gd_{0.1}$) $O_{2.02}$, ($U_{0.8}$ $Gd_{0.2}$) $O_{2.00}$, and ($U_{0.5}$ $Gd_{0.5}$) $O_{1.98}$ as a function of temperature in the temperature range 298 – 1973 K are shown in Figure 6 and are also listed in Table 8. The variation of lattice parameter, a (nm) with temperature (K) for ($U_{0.9}$ $Gd_{0.1}$) $O_{2.02}$, ($U_{0.8}$ $Gd_{0.2}$) $O_{2.00}$, and ($U_{0.5}$ $Gd_{0.5}$) $O_{1.98}$ is fitted to a second order polynomial in the temperature interval (T-298) by a least squares method and are given by the following expressions,

TABLE 7: HTXRD data of UO_2 and Gd_2O_3

T(K)	UO_2			Gd_2O_3		
	a (nm)	TE (%)	α (10^{-6} K^{-1})	a (nm)	TE (%)	α (10^{-6} K^{-1})
298	0.5470	0.00	7.69	0.5396	0.00	3.78
373	0.5473	0.06	8.09	0.5397	0.03	4.10
473	0.5478	0.14	8.61	0.5400	0.07	4.53
573	0.5482	0.23	9.14	0.5402	0.12	4.96
673	0.5488	0.33	9.67	0.5405	0.17	5.38
773	0.5493	0.42	10.20	0.5408	0.23	5.81
873	0.5499	0.53	10.72	0.5411	0.29	6.24
973	0.5505	0.64	11.25	0.5415	0.35	6.67
1073	0.5511	0.75	11.78	0.5418	0.42	7.09
1173	0.5518	0.87	12.31	0.5422	0.49	7.52
1273	0.5524	1.00	12.83	0.5427	0.57	7.95
1373	0.5532	1.13	13.36	0.5431	0.65	8.38
1473	0.5539	1.27	13.89	0.5436	0.74	8.80
1573	0.5547	1.41	14.41	0.5441	0.83	9.23
1673	0.5555	1.56	14.94	0.5446	0.92	9.66
1773	0.5563	1.71	15.47	0.5451	1.02	10.09
1873	0.5572	1.87	16.00	0.5456	1.13	10.51
1973	0.5581	2.03	16.52	0.5462	1.23	10.94

$$a\ (\text{nm})\ [(U_{0.9}\ Gd_{0.1})\ O_{2.02}] = 0.54523 + 3.1149 \times 10^{-6}\,(T - 298) + 1.4154 \times 10^{-9}\,(T - 298)^2 \quad (298 - 1973) \qquad (10)$$

$$a\ (\text{nm})\ [(U_{0.8}\ Gd_{0.2})\ O_{2.00}] = 0.54435 + 3.2626 \times 10^{-6}\,(T - 298) + 1.2673 \times 10^{-9}\,(T - 298)^2 \quad (298 - 1973) \qquad (11)$$

$$a\ (\text{nm})\ [(U_{0.5}\ Gd_{0.5})\ O_{1.98}] = 0.54253 + 2.3244 \times 10^{-6}\,(T - 298) + 1.2917 \times 10^{-19}\,(T - 298)^2 \quad (298 - 1973). \qquad (12)$$

Equations 10, 11, and 12 are used to calculate the mean linear thermal expansion of the respective mixed oxides and are presented in Table 8. From the variation of lattice parameters with temperature, % linear thermal expansion was computed and fitted to the following polynomial in temperature by a least squares method,

$$\text{TE (\%) } [(U_{0.9}\ Gd_{0.1})\ O_{2.02}] = -0.1922 + 5.7020 \times 10^{-4}\,T + 2.5910 \times 10^{-7}\,T^2 \quad (298 - 1973) \qquad (13)$$

$$\text{TE (\%) } [(U_{0.8}\ Gd_{0.2})\ O_{2.00}] = -0.1985 + 5.9742 \times 10^{-4}\,T + 2.2519 \times 10^{-7}\,T^2 \quad (298 - 1973) \qquad (14)$$

$$\text{TE (\%) } [(U_{0.5}\ Gd_{0.5})\ O_{1.98}] = -0.1985 + 4.2780 \times 10^{-4}\,T + 2.377 \times 10^{-7}\,T^2 \quad (298 - 1973). \qquad (15)$$

4. Discussion

As can be seen in Figure 3 representing the measured heat capacity data of ($U_{0.9}$ $Gd_{0.1}$) $O_{2.02}$, there is considerable anomalous increase in the heat capacity in the region above 550 – 600 K. Inaba et al[7] observed the same phenomenon for ($U_{0.899}$ $Gd_{0.101}$) $O_{2.001}$ in the region above 800 K, whereas Takahashi et al[14] have found no appreciable anomaly in the heat capacity curve up to 1500 K for nearly the same composition. Arita et al[8] have measured the heat capacities of UO_2 doped with Pr, Zr, and Ce, in which uranium predominantly exists as a tetravalent

TABLE 8: HTXRD data of urania- gadolinia solid solution

T(K)	$(U_{0.9}\ Gd_{0.1})\ O_{2.02}$			$(U_{0.8}\ Gd_{0.2})\ O_{2.00}$			$(U_{0.5}\ Gd_{0.5})\ O_{1.98}$		
	a (nm)	TE (%)	α (10^{-6} K^{-1})	*a* (nm)	TE (%)	α (10^{-6} K^{-1})	*a* (nm)	TE (%)	α (10^{-6} K^{-1})
298	0.5463	0.00	7.25	0.5454	0.00	7.32	0.5433	0.00	5.70
373	0.5466	0.06	7.63	0.5457	0.06	7.60	0.5436	0.04	6.05
473	0.5470	0.14	8.15	0.5462	0.13	8.08	0.5439	0.11	6.53
573	0.5475	0.22	8.67	0.5466	0.22	8.55	0.5443	0.17	7.00
673	0.5480	0.31	9.19	0.5471	0.31	9.03	0.5447	0.25	7.48
773	0.5485	0.40	9.71	0.5476	0.40	9.51	0.5451	0.32	7.95
873	0.5490	0.50	10.23	0.5481	0.49	9.99	0.5455	0.41	8.43
973	0.5496	0.61	10.74	0.5487	0.60	10.46	0.5460	0.49	8.91
1073	0.5502	0.72	11.26	0.5493	0.70	10.94	0.5465	0.58	9.38
1173	0.5508	0.83	11.78	0.5499	0.81	11.42	0.5470	0.68	9.86
1273	0.5515	0.95	12.30	0.5505	0.93	11.90	0.5476	0.78	10.33
1373	0.5522	1.08	12.82	0.5511	1.05	12.38	0.5482	0.89	10.81
1473	0.5529	1.21	13.34	0.5518	1.17	12.85	0.5488	1.00	11.28
1573	0.5536	1.35	13.85	0.5525	1.30	13.33	0.5494	1.11	11.76
1673	0.5544	1.49	14.37	0.5532	1.43	13.81	0.5500	1.23	12.23
1773	0.5552	1.63	14.89	0.5540	1.57	14.29	0.5507	1.36	12.71
1873	0.5560	1.78	15.41	0.5548	1.71	14.76	0.5514	1.49	13.19
1973	0.5563	1.94	15.93	0.5556	1.86	15.24	0.5521	1.62	13.66

state. They did not observe anomalous increase in the heat capacity up to 1410 K. Also, in our previous work[21] on the measurement of heat capacity of $(U_{1-y}\ Ce_y)\ O_2$, no such anomalous increase in the heat capacity was observed. Inaba et al[7] and Matsui et al[9,10] measured heat capacity of UO_2 doped with trivalent cations such as Gd, La, and Eu and observed that the onset temperature of the the heat capacity anomal decreases with increase in the dopant concentration. Matsui et al[10,11] also measured the electrical conductivity of these mixed oxide materials and observed, however, that the temperatures at which the slope of the conductivity curve changes is independent of the dopant and is close to the undoped UO_2. Also, the temperature at which the slope changes in the electrical conductivity curve did not coincide with the onset temperature of the heat capacity anomaly. Therefore, Matsui et al ruled out the formation of electron-hole pair being the cause for the heat capacity anomaly. Instead, he attributed it to the formation of Frenkel-pair like defects of oxygen. The present observed heat capacity anomaly might also be due to predominant contribution of formation of Frenkel pairs of oxygen. This is because the formation of large number of Frenkel-pair defects of oxygen is enabled when UO_2 is doped with aliovalent cations (M^{3+} in this case).[7-11] Arita et al[8] suggested that doping of trivalent cations to UO_2 produces greater complexity of oxygen arrangements, which in turn induces the formation of oxygen defects resulting in the heat capacity anomaly. The lower onset temperature of the heat capacity anomaly in the present measurement for $(U_{0.9}\ Gd_{0.1})\ O_{2.02}$ compared to that of Inaba et al[7] for nearly the same composition ($(U_{0.899}\ Gd_{0.101})\ O_{2.001}$ may be due to the larger non-stoichiometry of the present sample compared to that of Inaba et al.[7] The baseline heat capacity of $(U_{0.9}\ Gd_{0.1})\ O_{2.02}$ was obtained from a least squares fitting for the data in the low temperature region (298 to 500 K) and extrapolated up to 800 K. The difference between the baseline heat capacity and that of the measured data (ΔC_p) is plotted against temperature for all the solid solution in Figure 8. As can be seen in Figure 8, the onset of the heat capacity anomaly starts in the region of 550 – 600 K for $(U_{0.9}\ Gd_{0.1})\ O_{2.02}$.

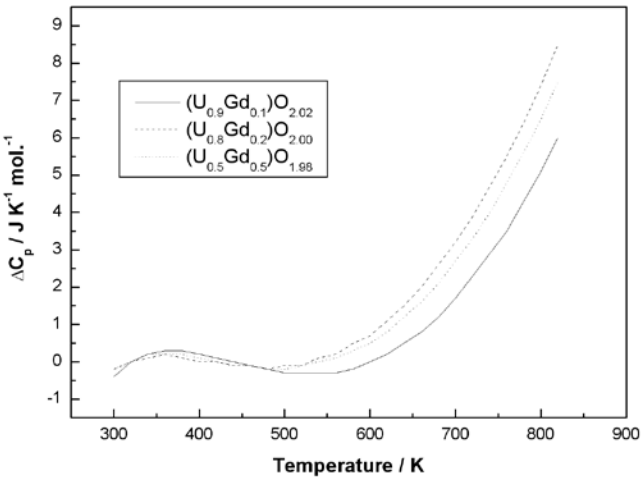

Figure 8. Difference between the baseline and measured heat capacity data (ΔC_p) vs *T* of (y = 0.1, 0.2, 0.5, and 0.8).

Heat capacity data of $(U_{1-y}\ Gd_y)\ O_{2\pm x}$ ($y \geq 0.2$) available in the literature are very less. The only measured heat capacity data are from Amaya et al[12,13] on $(U_{0.792}\ Gd_{0.208})\ O_2$ and $(U_{0.729}\ Gd_{0.271})\ O_2$. The present data is the first of the kind on the heat capacity of $(U_{1-y}\ Gd_y)\ O_{2\pm x}$ ($y \geq 0.271$). As can be seen in Figures 4 and 5 representing the measured heat capacity data of $(U_{0.8}\ Gd_{0.2})\ O_{2.00}$ and $(U_{0.5}\ Gd_{0.5})\ O_{1.98}$ respectively there is considerable anomalous increase in the heat capacity values in the region between 500 – 550 K. The heat capacity of $(U_{0.792}\ Gd_{0.208})\ O_2$ measured by Amaya et al is also shown in Figure 4 for comparison. As can be seen in Figure 4, unlike the present measurement on heat capacity of $(U_{0.8}\ Gd_{0.2})\ O_{2.00}$, Amaya et al did not observe any anomalous thermal effects for nearly the same composition $(U_{0.792}\ Gd_{0.208})\ O_2$. As observed by Inaba et al[7] and Matsui et al[9,10] there is decrease in the onset temperature of the heat capacity anomaly with the increase in dopant concentration. This observation is also shown in Figure 8.

However, the magnitude of the decrease in the onset temperature of the heat capacity anomaly as a function of dopant concentration is not as steep as that observed by Inaba et al. Also, in the present measurement it is observed that there is no decrease in the onset temperature of the heat capacity anomal for $(U_{1-y}\ Gd_y)\ O_{2\pm x}$ when y is increased from 0.2 to 0.5.

If E_d is the energy needed to form a defect, the number of defects n_d at any temperature T will be given by a Boltzmann factor

$$n_d = n_0 \exp(-E_d/kT) \quad (16)$$

and the specific heat of formation of such defects will be

$$\Delta C_v = d/dT(n_d E_d) = n_0 E_d^2/kT^2 \exp(-E_d/kT) \quad (17)$$

Thus, a plot of $\ln(T^2\Delta C_v)$ against $1/T$ is a straight line with a slope of $-E_d/k$. Similarly, a plot of $\ln(T^2\Delta C_p)$ against $1/T$ is a straight line with a slope of $-\Delta H_d/k$, where ΔH_d is the enthalpy of formation of the defect. The plot of $\ln(T^2\Delta C_p)$ against $1/T$ for $(U_{0.9}\ Gd_{0.1})\ O_{2.02}$, $(U_{0.8}\ Gd_{0.2})\ O_{2.00}$, and $(U_{0.5}\ Gd_{0.5})\ O_{1.98}$ in the temperature range 600 – 800 K is given in Figure 9. The ΔH_d determined from the slope of the plots for $(U_{0.9}\ Gd_{0.1})\ O_{2.02}$, $(U_{0.8}\ Gd_{0.2})\ O_{2.00}$, and $(U_{0.5}\ Gd_{0.5})\ O_{1.98}$ are 78.5 kJ mol^{-1} (0.813 eV), 54.5 kJ mol^{-1} (0.565 eV), and 58.0 kJ mol^{-1} (0.601 eV), respectively. The ΔH_d determined in the present study for $(U_{0.9}\ Gd_{0.1})\ O_{2.02}$ is in the same range as that computed by Inaba et al[7] (71.2 kJ mol^{-1}, 0.738 eV) for the nearly same composition $(U_{0.899}\ Gd_{0.1.01})O_{2.001}$. Inaba et al[7] also observed decrease in the ΔH_d with increase in Gd content for their measurement on $(U_{1-y}\ Gd_y)\ O_{2\pm x}$ upto $y = 0.142$. The ΔH_d for $y = 0.142$ of Inaba et al[7] is 53.3 kJ mol^{-1} (0.552 eV). The determined ΔH_d from the present measurement on $y = 0.2$ and 0.5 are 0.565 eV and 0.601 eV. Therefore, the present observation suggests that the decrease in the ΔH_d with Gd content reaches plateau for Gd content greater than 15%. The slight increase in the ΔH_d values for $y = 0.5$ may be due to the extrapolation and fitting errors.

The heat capacity of $(U_{1-y}\ Gd_y)\ O_{2\pm x}$ decreases with increase in y from 0.1 to 0.2. Amaya et al[13] attributed the phenomenon due to the decrease in the contribution of U^{4+} to excess heat capacity.[13] However, we consider that, with the increase in the concentration of trivalent dopant Gd, wherein heavier uranium atoms is replaced by lighter Gd atoms in UO_2 lattice as well as, U^{4+} is getting oxidized to higher oxidation states such as U^{5+} or U^{6+} to maintain electrical neutrality. Therefore, the phonon frequencies of $(U_{1-y}\ Gd_y)\ O_{2\pm x}$ are expected to be higher than that of UO_2 leading to lower heat capacity. But, the present heat capacity value of $(U_{1-y}\ Gd_y)\ O_{2\pm x}$ with $y = 0.5$ is higher than that of $y = 0.2$ at temperatures below 400 K and lower than that of $y = 0.2$ at temperatures above 400 K. Amaya et al[13] observed that the measured heat capacity data of $(U_{1-y}\ Gd_y)\ O_{2\pm x}$ tend to decrease with increasing y up to $y = 0.208$ and increase for $y = 0.271$. Amaya et al[13] suggested that the excitation conditions of the electrons might change with samples containing $y > 0.2$ compared to that of the samples having lower Gd concentrations because of the low concentration of U^{4+} ions (<50%). However, in the present measurement the heat capacity values of $(U_{1-y}\ Gd_y)\ O_{2\pm x}$ with $y = 0.5$ are lower than that of $y = 0.2$ at temperatures above 400 K. This may be explained by the reason that the influence of oxidation of U^{4+} ions on the decrease in heat capacity overwhelms that of change in excitation conditions of the electrons suggested by Amaya et al[13] at temperatures above 400 K.

As can be seen in Figure 10, the room temperature lattice parameter (a) of $(U_{1-y}\ Gd_y)\ O_{2\pm x}$ decrease with increase in dopant concentration. The ionic radius of U^{4+} with eightfold coordination is 0.1001 nm and that of Gd^{3+} is 0.1053 nm.[35] Though the smaller U^{4+} is substituted with larger Gd^{3+} ion there is decrease in the room temperature lattice constant with increase

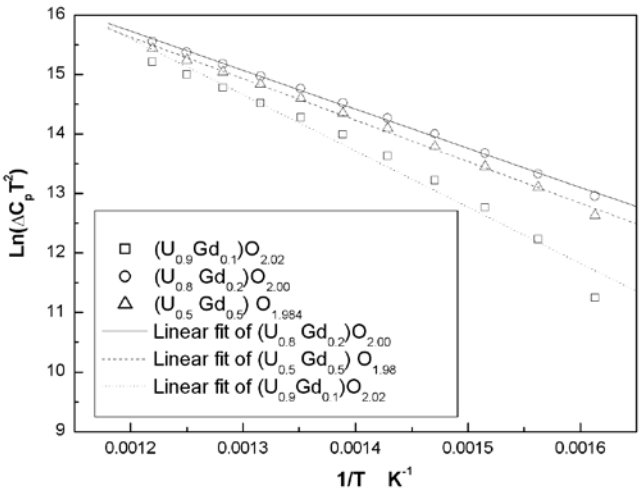

Figure 9. plot of $\ln(T^2\Delta C_p)$ vs $1/T$ in the temperature range 600 – 800 K.

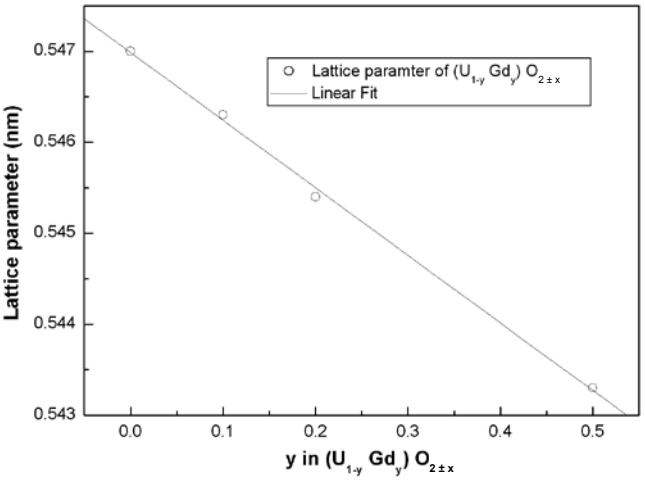

Figure 10. Variation of room temperature lattice constant as a function of Gd concentration.

in Gd content in the solid solution. This is because when U^{4+} is substituted with Gd^{3+} in the UO_2 lattice some of the U^{4+} is oxidized to either U^{5+} or U^{6+} in order to maintain electrical neutrality. The ionic radius of U^{5+} with eight fold co-ordination is 0.088 nm[36] and that of U^{6+} is 0.086 nm.[35] Therefore, the increase in lattice constant expected by doping of cation with larger ionic radius is overwhelmed by decrease in the average ionic radius of uranium ions due to oxidation, assuming a random distribution of the cations in the cation sub lattice. Therefore, a net negative change in the lattice constant on increase in dopant concentration is observed. Ohmichi et al[36] computed the da/dy of UO_2 doped with Gd based on the assumption that the U^{4+} oxidizes entirely to U^{5+} (da/dy = -0.0173 nm for Gd) or entirely to U^{6+} (da/dy = -0.0042 nm). Omichi et al[36] also measured room temperature lattice constant of UO_2 doped with Gd up to 15 at. % and observed that the measured da/dy (- 0.0173 nm) is close to that predicted with U^{4+} oxidized entirely to U^{5+}. The da/dy in the present measurement is -0.00743 nm, which suggests that U^{4+} may be oxidized both to U^{5+} and U^{6+}, but predominantly to U^{6+} on doping Gd^{3+}.

5. Summary

1. Four solid solution of urania-gadolinia mixed oxides were synthesized by combustion synthesis. Chemical compositions were determined by HPLC and ICP-AES. The structural characterization was done using XRD.

2. Single phase fluorite structure was observed for $(U_{1-y}\ Gd_y)\ O_{2\pm x}$ ($y = 0.1 - 0.5$) and for $(U_{0.2}\ Gd_{0.8})\ O_{1.71}$ additional faint hexagonal gadolinia lines were observed.
3. The room temperature lattice constant (a) of $(U_{1-y}\ Gd_y)\ O_{2\pm x}$ ($y = 0.1 - 0.5$) decreases linearly with y. The slope da/dy suggests that U^{4+} in the UO_2 lattice is oxidized predominantly to U^{6+} on doping with Gd to maintain electrical neutrality.
4. Molar heat capacities were measured for $(U_{1-y}\ Gd_y)\ O_{2\pm x}$ ($y = 0.1 - 0.5$) by differential scanning calorimetry in the temperature region 298 – 800 K.
5. Considerable anomalous increase in the heat capacity were observed for $(U_{1-y}\ Gd_y)\ O_{2\pm x}$ with $y = 0.2$ to 0.5. Also, it was observed that the onset temperature of the anomalous increase in the heat capacity decreases with the increase in Gd content and the above behaviour is attributed to formation of Frenkel pair like defects of oxygen.
6. The enthalpy of defect formation ΔH_d determined from the present measurement for $(U_{1-y}\ Gd_y)\ O_{2\pm x}$ ($y = 0.1$) is in the same range that determined by Inaba et al[7] for nearly same composition.
7. The ΔH_d values decrease with increase in Gd content for $(U_{1-y}\ Gd_y)\ O_{2\pm x}$ up to $y = 0.15$ and remains constant for higher concentrations of Gd.
8. Thermal expansion measurements were carried out on $(U_{1-y}\ Gd_y)\ O_{2\pm x}$ ($y = 0.1 - 0.5$) in the temperature range 298 – 1973 K. There are no thermal expansion data of urania-gadolinia mixed oxide and the present data is the first of the kind.

References

(1) R.A. Hein, P.N. Flagella, and J.B. Conway, J. Am. Ceram. Soc. **51**, 291 (1968).
(2) J.F. Kerrisk and D.G. Clifton, Nucl. Technol. **16**, 531 (1972).
(3) R. Szwarc, J. Phys. Chem. Solids **30**, 705 (1969).
(4) J.H. Harding, P. Masri, and A.M. Stoneham, J. Nucl. Mater. **92**, 73 (1980).
(5) J. Ralph and M.J. Gillan, J. Nucl. Mater. **126**, 111 (1984).
(6) R.A. Young, J. Nucl. Mater. **87**, 283 (1979).
(7) H. Inaba, K. Naito, and M. Oguma, J. Nucl. Mater. **149**, 341 (1987).
(8) Y. Arita, T. Matsui, and S. Hamada, Thermochim. Acta **253**, 1 (1995).
(9) T. Matsui, Y. Arita, and K. Naito, J. Radioanal. Nucl. Chem. **143**, 149 (1991).
(10) T. Matsui, T. Kawase, and K. Naito, J. Nucl. Mater. **186**, 254 (1992).
(11) T. Matsui, Y. Arita, and K. Naito, J. Nucl. Mater. **188**, 205 (1992).
(12) M. Amaya, K. Une, and K. Minato, J. Nucl. Mater. **294**, 1 (2001).
(13) M. Amaya, K. Une, and M. Hirai, J. Nucl. Sci. Technol. **41**, 108 (2004).
(14) Y. Takahashi and M. Asou, J. Nucl. Mater. **201**, 108 (1993).
(15) JCPDS Card No. 41-1422
(16) JCPDS Card No. 73-2403
(17) JCPDS Card No. 24-0430
(18) R.J. Beals, J.H. Handwerk, and B.J. Wrona, J. Am. Ceram. Soc. **52**, 578 (1969).
(19) E.A. Aitken, S.F. Bartram, and E.F. Juenke, Inorg. Chem. **3**, 949 (1964).
(20) S. Kihara, T. Adachi, and H. Hashitani, Fresenius Z. Anal. Chem. **303**, 28 (1980).
(21) R.V. Krishnan and K. Nagarajan, Thermochim. Acta **440**, 141 (2006).
(22) L.B. Pankratz, *Thermodynamic Properties of oxides*, Bull. US Bur. Mines, 1984.
(23) R.J.M. Konings, J.C. van Miltenburg, and A.C.G. van Genderen, J. Chem. Thermodyn. **37**, 1219 (2005).
(24) J.K. Fink, J. Nucl. Mater. **279**, 1 (2000).
(25) K.C. Mills, R.H. Ponsford, and M.J. Richardson, Thermochim. Acta, **139**, 107 (1989).
(26) A.C. Momin and M.D. Karkhanavala, High Temp. Sci. **10**, 45 (1978).
(27) M. Hoch and H.L. Johnston, J. Phys. Chem. **65**, 1184 (1961).
(28) K. Bakker, E.H.P. Cordfunke, R.J.M. Konings, and R.P.C. Schram, J. Nucl. Mater. **250**, 1 (1997).
(29) B. Skinner, Am. Miner. **42**, 39 (1957).
(30) C.P. Kempter and R.E. Elliott, J. Chem. Phys. **30**, 1524 (1958)
(31) M. Hoch and A.C. Momin, High Temp. High Press. **1**, 401 (1969).
(32) Touloukian, *Thermal Expansion: Non Metallic Solids*, IFI, Plenum, New York, 1970.
(33) A.C. Momin, E.B. Mirza, and M.D. Mathews, J. Nucl. Mater. **185**, 308 (1991).
(34) JJ.Belle and R.M. Berman, P*roperties and Nuclear applications* DOE/NE-0060, 1984.
(35) R. D. Shannon, Acta. Cryst. A. **32**, 751 (1976).
(36) T. Ohmichi, S. Fukushima, A. Maeda, and H. Watanabe, J. Nucl. Mater. **102**, 40 (1981).